Int J Adv Manuf Technol (2016) 87:2615–2623
DOI 10.1007/s00170-016-8633-1

ORIGINAL ARTICLE

Effects of thermal cycles on microstructure evolution of 2219-Al during GTA-additive manufacturing

J. Y. Bai[1] · C. L. Fan[1] · S. b. Lin[1] · C. L. Yang[1] · B. L. Dong[1]

Received: 5 November 2015 / Accepted: 17 March 2016 / Published online: 31 March 2016

Abstract A 2219-Al thin-walled component was produced by gas tungsten arc (GTA)-additive manufacturing, and the microstructures were observed. The thin wall can be divided into two regions: a top region and a bottom region. In the top region, dendritic structures dominate and the eutectics are discontinuous. In the bottom region, there are many light strips dividing the region into parallel layers. In this region, dendritic structures are absent and eutectics are continuous. During the GTA-additive manufacturing process, deposited materials are heated many times by thermal cycles. According to consequences and time sequences, thermal cycles can be classified into three categories: melting heat, partial-melting heat, and post-heat. The top region is the melting-heat-affected zone, whose microstructures are the consequences of the melting heat. The line between the top region and bottom region is the partial-melting-affected zone, whose microstructures are affected by melting heat and by partial-melting heat. As for the post-heat-affected zone, namely the bottom region, melting heat and post-heat contribute to the inner-layer parts' microstructures, while melting heat, partial-melting heat, and post-heat contribute to the inter-layer line microstructures together.

Keywords Additive manufacturing · 2219-Al · Microstructure evolution · Thermal cycles

✉ S. b. Lin
sblin@hit.edu.cn

[1] State Key Laboratory of Advanced Welding and Joining, Harbin Institute of Technology, Harbin 150001, China

1 Introduction

Additive manufacturing (3D printing) is a type of rapidly developing and promising technology. Usually, it uses high-energy-density beams as heat sources, such as laser beams and electron beams. Recently, researchers have found that sources of electric arcs have many advantages over high-energy-density beams, referring to their efficiency and economy [1–5]. Gas tungsten arc (GTA)-additive manufacturing is a kind of arc-source additive manufacturing technology, which uses the heat of the typical gas tungsten arc welding (GTAW) arc to melt materials. With simple welding equipments, components of various kinds of materials have been produced, such as TC4, Inconel625, 308L steel, 300M steel, and 5356-Al [6–12].

During the additive manufacturing process, materials in components are deposited layer by layer. As a result, the deposited materials have to be heated many times (except for the last deposited layer). As a result, the microstructures of the additive manufactured materials have some differences from the conventionally produced materials. For example, Baufeld reported that there were two kinds of strips in the TC4 components. Additionally, the columnar grains in TC4 were so big that they can be macroscopically observed [6]. However, in the research of steels, only one type of strips was found in 308L steel and 300M steel by Skiba [8, 9]. As for the study of Inconel625, Fujia Xu declared that the segregation phenomenon was a significant matter in microstructures, which directly influences the mechanical properties [7]. Wang produced a 5356-Al cylinder and observed from bottom to top, finding the microstructures transforming from columnar grains to equiaxed grains [10]. Similarly, Liu produced some 5356-Al components with CMT. There were many columnar grains in the inter-layer lines. Controlling the temperature during manufacturing can achieve fine grains [12]. After years of

research, many achievements about microstructure observation have been obtained. But the relationship between the thermal process and microstructure evolution has not been thoroughly understood. In the current study, the microstructures of the additive manufactured 2219-Al are observed. And most importantly, the effects of the thermal cycles on microstructure evolution are carefully analyzed.

2 Experimental

Experiments are carried out on an experimental setup, which is shown in Fig. 1. In this setup, a CLOSS GLW300 power supply is used, a GTAW gun is tied to the moving tables, and a preheat table is used to heat the base plate. ER2319 wire is the feeding material and the diameter is 1.2 mm. The material 2319 is designed especially for the welding of 2219-Al. The chemical constituents of 2319-Al and 2219-Al are identical (nominally Al-6 wt% Cu), except for a slight variation of Ti. In this paper, the additive manufactured material will be referred to as 2219-Al, because this is the common alloy designed for product forms other than weld-feeding wire.

A thin-wall component is produced in this paper. In the first layer, the arc is maintained between the tungsten electrode and the base plate, while in other layers, the arc is maintained between the tungsten electrode and the last beam. In each layer, the beam is deposited from the same side and the wire is fed in front of the arc. When the beam deposition of one layer is finished, the arc will be extinguished and the welding gun will be raised by a certain distance. In order to avoid overheating, the resident temperature of the last beam is detected, and the next beam will not be deposited until the resident temperature reaches that fixed value. The additive manufactured thin wall is shown in Fig. 2, and the welding parameters and dimensions of the thin wall are given in Table 1. It should be noted that, in order to keep the width of the beams the same, the first few layers need a higher heat input, but these parameters are not given in this paper. Some metallographic specimens are made from the cross sections of different heights. After grinding and polishing, the specimens are etched with Keller's reagent for 3 s. Finally, an optical microscope and a scanning electron microscope (SEM) are used to observe the microstructures.

Fig. 1 GTA-additive manufacturing system

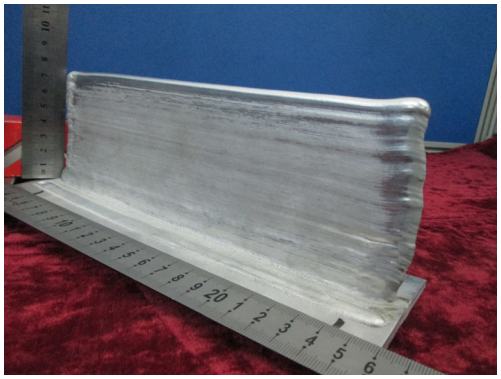

Fig. 2 Thin-walled component

3 Microstructures

Figure 3 is the etched cross section of the thin wall approaching the top. There are two regions in the cross section, and they are the top region and the bottom region. The area of the top region is smaller and the profile is a semi-circle. The rest area of the thin wall belongs to the bottom region which is rectangular in shape. The outline is smooth and the signs between the deposited layers are difficult to be defined. The color of the top region is much lighter than that of the bottom region. Simultaneously, there are many light stripes in the bottom region. These light stripes are parallel with each other and the distances between the stripes are almost the same. Parallel stripes divide the bottom region into parallel layers. In this paper, the light stripes are defined as inter-layer lines, and the spaces between the light stripes are defined as inner-layer parts.

The microstructures of the additive manufactured 2219-Al exhibit different characteristics in the top and bottom regions. Figure 4a is the dendritic structures in the top region, whose

Table 1 Welding parameters and dimensions of thin wall

Arc current (A)	103
Welding speed (mm/min)	200
Wire feeding speed (mm/min)	1000
Resident temperature (°C)	70–90
Arc length (mm)	3
Electrode diameter (mm)	2.4
Flow rate of shielding gas (L/min)	10
Length of thin wall (mm)	200
Thickness of thin wall (mm)	7.0
Height of thin wall (mm)	70

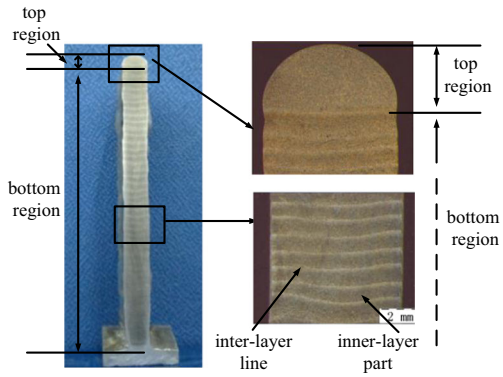

Fig. 3 Cross section of thin-wall

dendritic clearances and secondary dendritic arms can be easily uncovered. Since the grain boundaries and sub-boundaries are flourishing, grain boundaries are difficult to be uncovered. As a result, the sizes of the grains cannot be measured.

In the bottom region, the morphologies of the grains are more complicated. Grains of the inner-layer parts are shown in Fig. 4b. The equiaxed grains dominate in this part, while the dendritic structures are absent. The boundaries of the grains are clear, and the sizes of the grains are about 50 μm. Microstructures of the inter-layer lines (light strips) are shown in Fig. 6c. Although the equiaxed grains also dominate in these lines, the sizes of the grains are not homogeneous. There are many small fragments of broken grains, and thus, the amount of grain boundaries multiplies. It suggests that the increasing grain boundaries contribute to the light strips in the macroscopic structure. Additionally, some interesting phenomena can be obtained in the junction between the inner-layer part and inner-layer line, as shown in Fig. 4d. Although the area of the junction is narrow, the grain boundaries decrease sharply in the junction. It seems that the growth of the grains breaks in this junction. Meanwhile, there are some slender grains growing from the planer region. It should be noted that so far it is the first time to be reported that there is the phenomenon of decreasing grain boundaries in additive manufactured materials.

Eutectics in the top and bottom regions are also observed by SEM. Figure 5a is the top region, and eutectics of punctiform and claviform dominate. The eutectics in the grain boundaries and sub-boundaries are discontinuous. While in the bottom region, the distribution of the eutectics is continuous. Figure 5b is the inner-layer part, and latticed eutectics take the places of punctiform and claviform eutectics. Figure 5c is the inter-layer line, where the bulk of eutectics is much thicker. The width of the bulk eutectics can be tens of times as much as the latticed eutectics. As a phenomenon of grain boundaries, the amount of eutectics decreases sharply in the junction between the inner-layer part and the inter-layer line, as shown in Fig. 5d.

By increasing the microscope brightness to its maximum value, Fig. 6a is obtained. There are many small porosities in the cross section. Porosities exhibit a belt-like distribution in the inter-layer lines. The porosities can be classified into two categories: inner-smooth porosities and inner-rough porosities and are shown in panels b and c of Fig. 5, respectively. The sizes of the porosities are usually smaller than 50 μm.

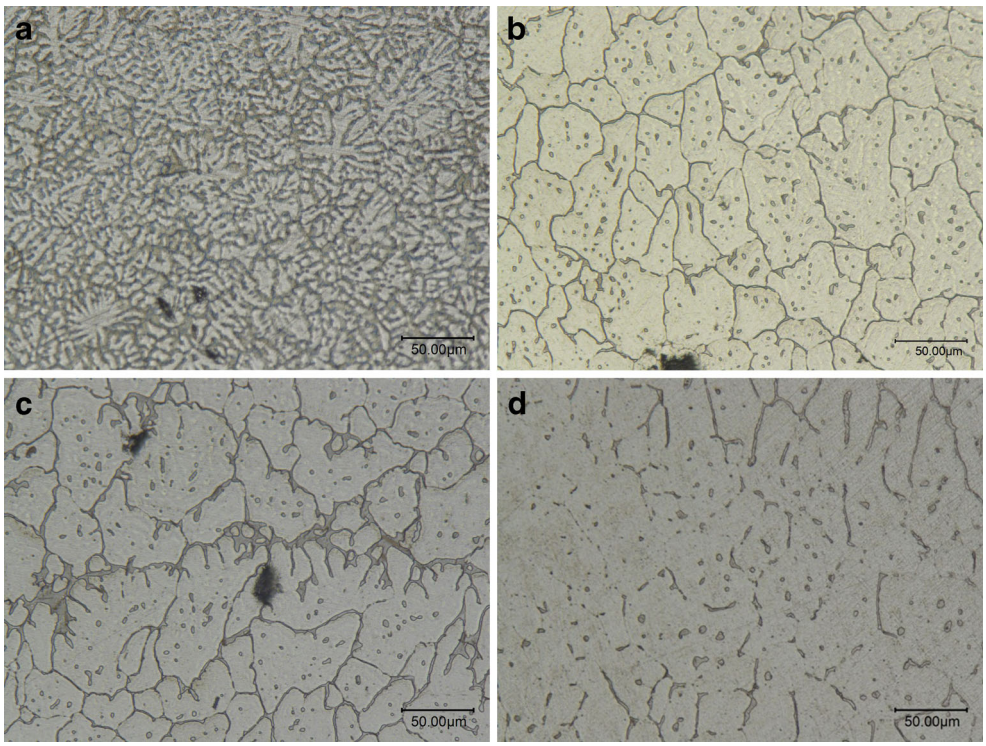

Fig. 4 Grains in additive manufactured 2219-Al. **a** Top region, **b** inner-layer part, **c** inter-layer line, **d** junction between inner-layer part and inter-layer line

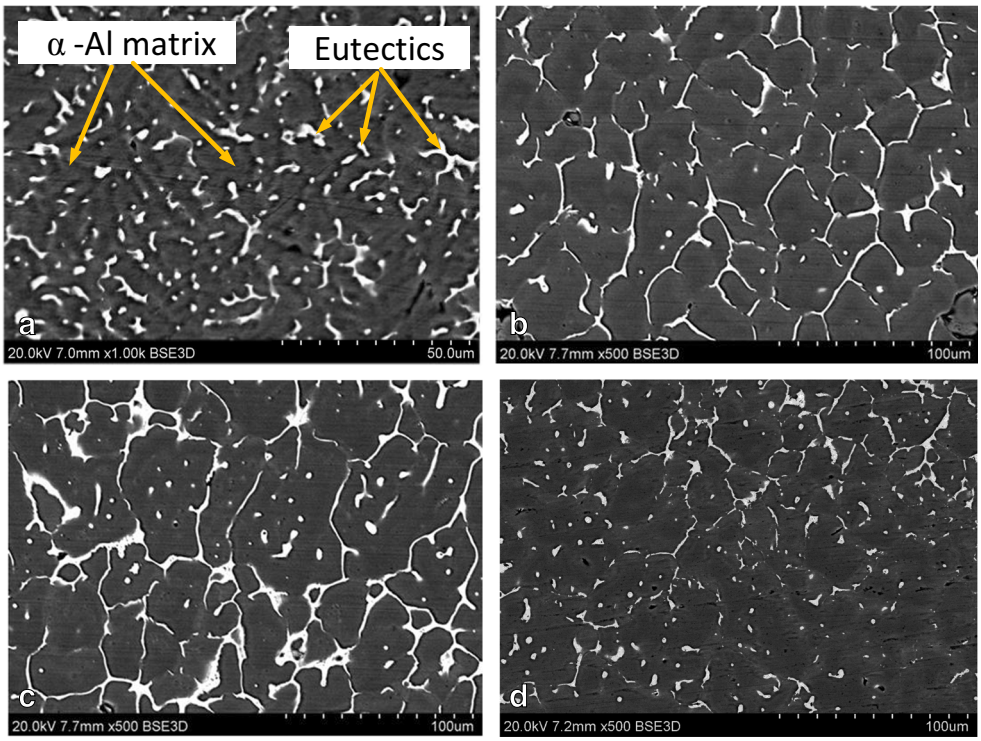

Fig. 5 Eutectics in additive manufactured 2219-Al. **a** Top region, **b** inner-layer part, **c** inter-layer line, **d** junction between inner-layer part and inter-layer line

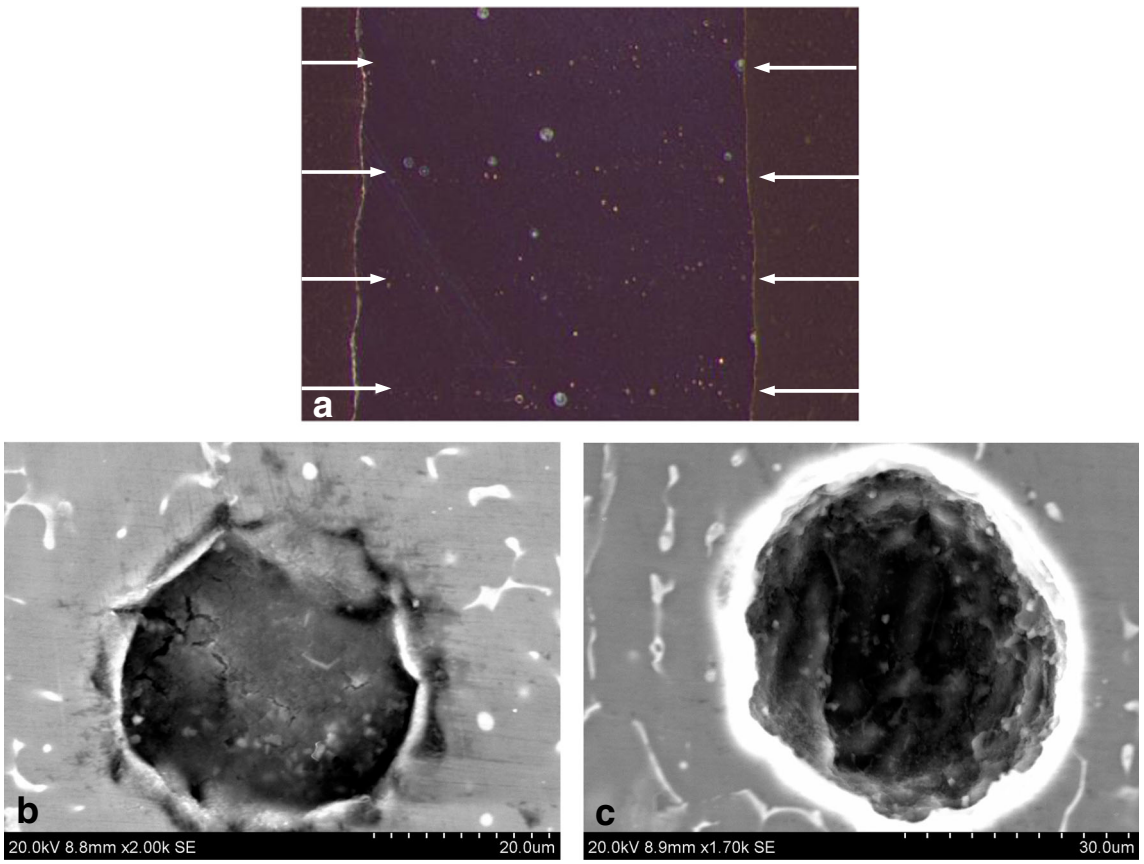

Fig. 6 Porosities in additive manufactured 2219-Al. **a** Belt-like distribution of porosities, **b** inner-smooth porosity, **c** inner-rough porosity

Generally speaking, porosities of this size can do little harm to the mechanical properties of the material. But taking into consideration the belt-like distribution, the results are not clear.

4 Effects of thermal cycles

4.1 Thermal cycles during GTA-additive manufacturing

Figure 7b is the thermal cycles of the P7 point. The P7 point is the middle point in both welding and building directions of the seventh layer. The thermal cycles are obtained by MSC.Marc, and details of the calculation are not shown in this paper. The material of P7 point has been heated seven times during manufacturing. The peak temperature of the first thermal cycle is the highest and it melts the wire. Peak temperatures of following thermal cycles decline gradually, as is shown in Fig. 7b. All the bottom temperatures of the thermal cycles are equal to the resident temperature, which is given in Table 1, and are about 80 °C.

Some conclusions can be obtained from Fig. 7a, b. During the last thermal cycle, the peak temperatures of the thermal cycles decline gradually from top to bottom. Thus, there must be a line between P3 and P4, whose peak temperature is 660 °C. Additionally, there must be a 548 °C peak temperature line between P4 and P5. If the temperature exceeds 660 °C (T_L, the melting point of α-Al), that means the point of the material is melted at this moment. If the temperature exceeds

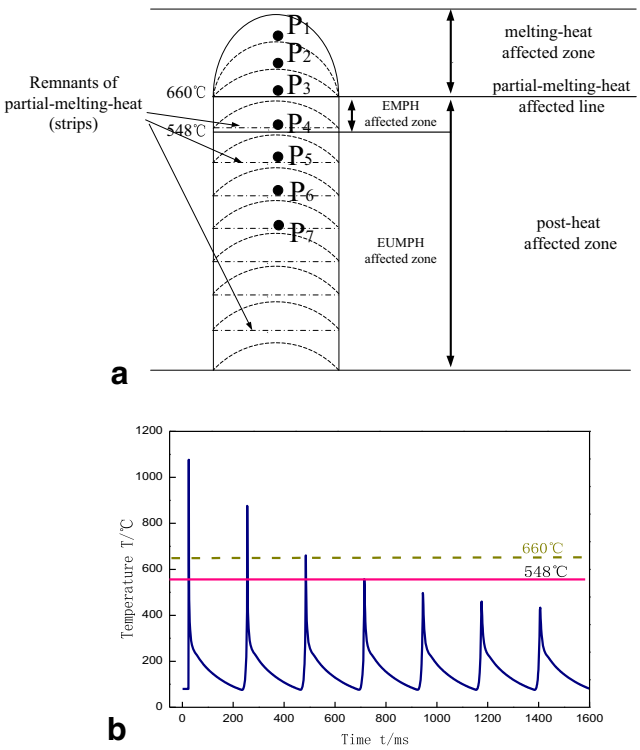

Fig. 7 Thermal cycles of P_7 point. **a** Sketch map of thin wall, **b** thermal cycles

548 °C (T_E, melting point of θ-Al_2Cu), that means the eutectic reaction is carried out: $\alpha + \theta \rightarrow L$, and the point of the eutectic is melted at this moment. As shown in Fig. 7b, there are three peaks exceeding T_L, which means P1, P2, and P3 points are melted during the last thermal cycle. Thus, the heat of the TIG arc can melt more than two layers deep in the thin wall during material deposition. As a conclusion, the top region consists of more than two layers amounting to the deposited material. However, as shown in Fig. 3, there is no line in the top region. That means the lines between the deposited materials cannot be seen in the additive manufactured 2219-Al. The conclusion proves that the light strips are fusion zones in the GTAW other than materials' deposition lines.

Thermal cycles during additive manufacturing are performed sequentially. According to the consequences and time sequences, they can be classified into three categories: melting heat when the peak temperature exceeds T_L, partial-melting heat when the peak temperature is equal to T_L, and post-heat when the peak temperature is less than T_L. The microstructures in the top region are the consequences of melting heat. At a certain point of the material, the melting-heat process is first performed and it is inevitable. Because of the layer height, a partial-melting-heat process is performed only for special points after the melting-heat process. The post-heat process is performed for all points of the materials. As shown in Fig. 7a, the top region is the melting-heat-affected zone, whose microstructures are the consequences of the melting heat. The line between the top region and bottom region is the partial-melting-affected line, where the microstructures are affected by melting heat and partial-melting heat. As for the post-heat-affected zone, namely the bottom region, the melting heat and post-heat contribute to the inner-layer part of the microstructures, while the melting heat, partial-melting heat, and post-heat contribute to the inter-layer line microstructures together.

4.2 Melting-heat process

For any point of the materials, the melting heat is performed at the beginning. In the melting-heat process, the materials of the feeding wire and some of the top layers are melted. In the following solidification process, planer grains are first formed at the bottom of the molten pool. But the growth of the planer grain is not stable. With the solidification of the liquid phase, the survival requirement of planer grains will break, which is given as follows [13]:

$$G \geq \frac{\Delta T}{D_L} R \tag{1}$$

where G represents the temperature gradient, R represents the growth rate, D_L represents the diffusion coefficient, and ΔT

represents the temperature difference between the solid and liquid interface.

As solidification is processed, segregation of the solutes becomes more and more serious, which leads to a temperature decreasing of solid-liquid equilibrium. As a result, the constitutional supercooling increases and the survival requirement of the planer grains breaks. At this time, cellular and columnar grains begin to form [14]. They grow along the building direction of the thin wall, because this direction has the best heat sink condition. When constitutional supercooling is high enough, equiaxed grains begin to form. Because the increasing rate of constitutional supercooling is so fast in the GTAW process, the junction area between planer grains and columnar grains is narrow. As a result, equiaxed grains will dominate the inner-layer part. The general growth frame of grains in GTAW is shown in Fig. 8. However, in fact, planer, columnar, and equiaxed grains are hard to be found in the melting-heat-affected zone. On the contrary, dendritic structures are flourishing. It is not the absence of them; actually, they are disturbed by the segregation of solutes, which will be analyzed in more detail later in this paper.

Another consequence of the melting-heat process is the segregation of solutes. Because the solidification rate is fast in GTAW, solutes have no time to completely diffuse.

In 2219-Al, eutectics consisted of θ-Al_2Cu and α-Al. However, during the formation of eutectics, α-Al in eutectics will unite with α-Al matrix. Thus, the main constituent of eutectics is θ-Al_2Cu. Since the melting point of α-Al is higher than that of θ-Al_2Cu, α-Al forms earlier in the liquid phase. The result is that interior places of the grains consist more of the Al element, while dendritic clearances and grain boundaries consist more of the Cu element [15], as shown in Fig. 9. The segregation of solutes is remarkable in that the dendritic structures are easy to be distinguished. As a result, planer, columnar, and equiaxed grains exhibit dendritic structures. At the end of solidification, the segregation is so serious that the eutectics ultimately form in grain boundaries and sub-

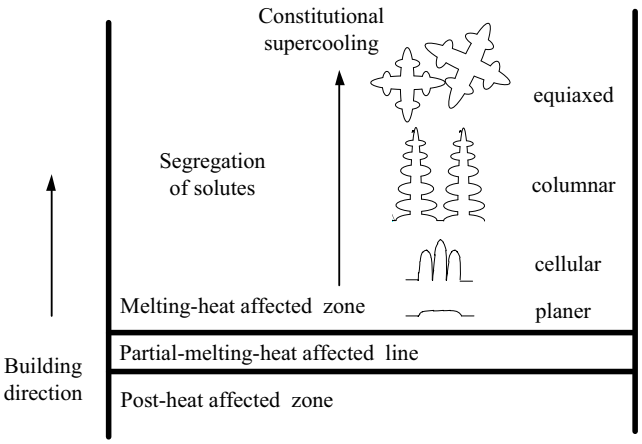

Fig. 8 Grain growth during melting-heat process

boundaries. But the content of Cu in the wire is 6.3 %, which is much lower than the value of eutectics (33.2 %). Thus, the insufficiency of content contributes to the discontinuous eutectics.

4.3 Partial-melting-heat process

As is described before, dendritic structures are clear and eutectics distribute in the grain boundaries after the melting-heat process. During the partial-melting-heat process, the peak temperature is equal to T_L. However, T_L is a stagnation temperature and it is only a transient process. In such condition, θ-Al_2Cu can melt completely, but the α-Al is only partially melted. As a result, some ends of dendritics are melted and the gaps between grains become wider. Since the liquid phase flows into the gaps, when the temperature cools down, the eutectics become bulky in shape. Meanwhile, fragments of broken dendritics ultimately result in many small grains, which increase the amount of grain boundaries. Actually, it is the increasing grain boundaries that contribute to the light strips (inter-layer lines) in the macroscopic structure.

Another consequence of the partial-melting-heat process is the re-distribution of solutes. According to Fick's first law, which is given in Eq. (2), the rate of element diffusion increases rapidly when temperature increases [16].

$$J = -D\frac{dC}{dx} \tag{2}$$

where J represents diffusion flux, D is the material coefficient, and dC/dx is the density gradient. As expressed in Eq. (2), J is in direct proportion to D. Thus, if D is obtained, J can be calculated. In the meantime, D can be expressed as follows [16]:

$$D = D_0 \exp\left(-\frac{Q}{RT}\right) \tag{3}$$

where D_0 represents the diffusion constant, Q represents the activation energy of diffusion, R represents the gas constant, and T represents the thermodynamic temperature.

In Eq. (3), D and T exhibit an exponential relationship. It reveals that, in contrast to T_R, the element diffusion rate in T_L increases exponentially. Because, at high temperatures, atoms vibrate more intensely. With the aid of energetic fluctuation, the probability for an atom to jump over the energy barrier is much larger in high temperatures. As a result, during this heat process, solutes are re-distributed. As is described before, the interior places of the dendritic structure are rich in Al, while the dendritic clearances and grain boundaries are rich in Cu. During the partial-melting-heat process, Al presents a downhill diffusion feature to reduce the density gradient. On the contrary, Cu presents an uphill diffusion feature, as shown in Fig. 10. Because, in the current conditions, α-Al is in a

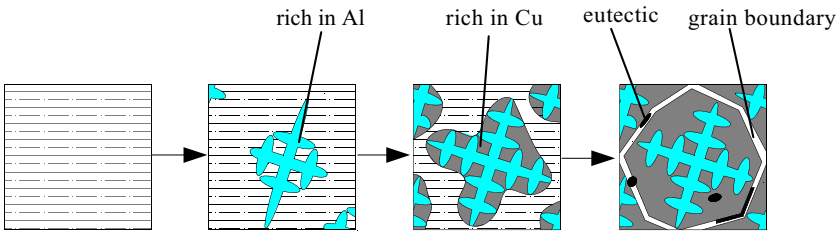

Fig. 9 Solute segregation during melting-heat process

supersaturated solid state, Cu has to separate out from α-Al. Meanwhile, in the grain boundaries, eutectic reactions can consume a large amount of Cu. Thus, Cu is segregated into grain boundaries. Since the segregation in dendritic clearances is alleviated after the partial-melting-heat process, the morphologies of dendritic structures are invisible. As a result, dendritic structures transform into equiaxed grains.

There is a kind of undesirable consequence of the partial-melting-heat process, which is the belt-like distribution of porosities in inter-layer lines. During the partial-melting process, broken dendrites and the fast solidification rate in GTAW together make the bottom of the melting pool where porosities can easily be formed in that position. The prior factor increases the probability of nuclei generation and the latter factor decreases their chance of escape. Generally, porosities in Al alloy belong to hydrogen pores [17, 18]. Since the whole of the thin wall is deposited by welding wire, the wire surfaces exist as a sufficient hydrogen element supply. Other research has proved this source theory. A thin wall was manufactured in a seal chamber, which was inflated by argon. In this condition, hydrogen was completely isolated. But the results showed that the amount of porosities did not decrease. Thus, the only possible source for the hydrogen is the wire surfaces.

4.4 Post-heat process

According to the effects on microstructure evolution, the post-heat can be classified into two categories: eutectic-melted post-heat (EMPH) when peak temperatures of the thermal cycles are higher or equal to T_E and eutectic-unmelted post-heat (EUMPH) when peak temperatures of the thermal cycles are lower than T_E. After the melting-heat and partial-melting-heat processes, the EMPH and EUMPH processes are performed sequentially.

During the EMPH process, the morphologies of the grains are immutable, but the eutectics can re-form. During this process, when the temperature reaches T_E, the eutectic reaction is carried out: $\alpha + \theta \rightarrow L$ and θ-Al_2Cu are melted. In this condition, the liquid phase flows like a river. Branches of the river merge with each other, joining the main stem in grain boundaries. However, during the EMPH process, the peak temperature is lower than T_L, and α-Al cannot be melted. When the temperature cools down to T_E again, the eutectics are re-formed. As a result, in the post-heat-affected zone, the eutectics are continuous. Although, some punctiform eutectics can survive during this process, their amount and sizes are much smaller. Additionally, re-distribution of solutes is also remarkable during the EMPH process, as it does in the partial-melting heat process. Segregation in dendritic clearances is alleviated, and the morphologies of dendritic structures are invisible. As a result, in post-heat-affected zones, the dendritic structures transform into planer, columnar, and equiaxed grains.

The EUMPH process is carried out after the EMPH process. Because the peak temperature is lower than the melting points of α-Al and θ-Al_2Cu, the morphologies of the grains and eutectics cannot transform any further. Additionally, at such temperature, element diffusion is not as remarkable as in the EMPH process. In fact, the EUMPH process has little effect on microstructure evolution.

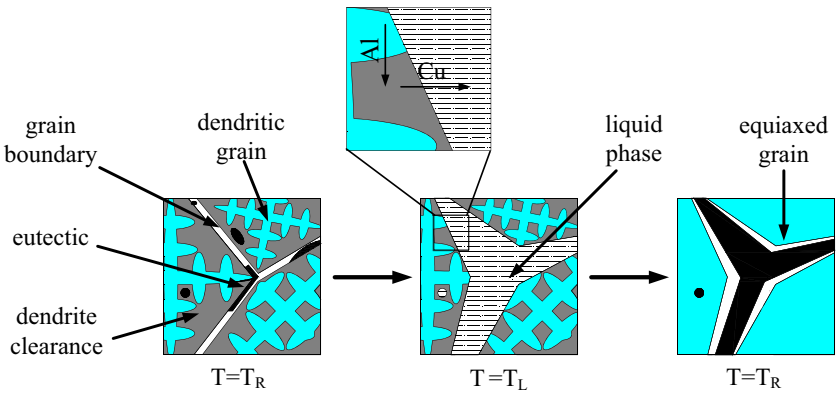

Fig. 10 Microstructure evolution during part-melting process

5 Conclusion

(1) The GTA-additive manufactured thin wall of 2219-Al can be divided into two regions: top region and bottom region. In the top region, grains exhibit a dendritic structure and the eutectics are discontinuous. In the bottom region, there are many light strips dividing the region into parallel layers. Each layer can be divided into the inner-layer parts and the inter-layer lines. The dendritic structure is absent in the whole bottom region. In the inner-layer part, equiaxed grains are dominant and eutectics are latticed. In the inter-layer line, there are many fragments of the equiaxed grains, which increases the amount of grain boundaries. At the junction between the inner-layer part and inter-layer line, the boundaries of the grains decrease sharply, and only some slender grains grow from the planer region.

(2) The deposited material has to be heated many times by thermal cycles during the additive manufacturing process. According to consequences and time sequences, thermal cycles can be classified into three categories: melting heat, partial-melting heat, and post-heat. The top region is the melting-heat-affected zone, whose microstructures are the consequences of the melting heat. The line between the top region and bottom region is the partial-melting-affected zone, whose microstructures are affected by melting heat and partial-melting heat. As for the post-heat-affected zone, namely the bottom region, the melting heat and post-heat contribute to the inner-layer parts of the microstructures, and melting heat, partial-melting heat, and post-heat contribute to the inter-layer line microstructures together.

(3) During the melting-heat process, materials of the wire and former layers are melted. In the solidification process, grains of planer, cellular, columnar, and equiaxed form successively. The increasing rate of constitutional supercooling is so fast that the area of the planer-columnar grains is narrow at the junction between the inner-layer part and inter-layer line. On a wider scale, equiaxed grains dominate. Because of the fast rate of solidification, solutes have no time to diffuse. Al is rich in the interior of the grains, while Cu is rich in the dendritic clearances and grain boundaries. So, the dendritic structures are clear in the top region.

(4) During the partial-melting-heat process, ends of the dendritics are broken. Fragments of the broken grains increase the amount of grain boundaries which contributes to the light strips in the macroscopic structure. Because the gaps between the grains become wider, the bulk of eutectics forms when the temperature cools down. Solute diffusion is especially remarkable in this process. Al presents a downhill diffusion feature to reduce the density gradient. On the contrary, Cu presents an uphill diffusion feature. Additionally, porosities are an unwanted consequence of this process.

(5) Post-heat can be classified into two categories: eutectic-melted post-heat (EMPH) and eutectic-unmelted post-heat (EUMPH). During the EMPH process, eutectics are re-formed and discontinuous eutectics become continuous. Segregation in dendritic clearances is alleviated, and dendritic structures transform into planer grains, columnar grains, and equiaxed grains. On the contrary, EUMPH process has little effect on microstructure evolution.

References

1. Clark D, Bache MR, Whittaker MT (2008) Shaped metal deposition of a nickel alloy for aero engine applications. J Mater Process Tech 203:439–448
2. Ding D, Pan Z, Cuiuri D, Li H (2015) Wire-feed additive manufacturing of metal components: technologies, developments and future interests. Int J Adv Manuf Techno 81:1–17
3. Xiong J, Zhang GJ (2014) Adaptive control of deposited height in GMA-based layer additive manufacturing. J Mater Process Tech 214:962–968
4. Aiyiti W, Zhao W, Lu B et al (2006) Investigation of the overlapping parameters of MPAW-based rapid prototyping. Rapid Prototyping J 12:165–172
5. Liu L, Zhuang Z, Liu F, Zhu M (2013) Additive manufacturing of steel–bronze bimetal by shaped metal deposition: interface characteristics and tensile properties. Int J Adv Manuf Technol 69:2131–2137
6. Baufeld B, Van der Biest O (2009) Mechanical properties of Ti-6Al-4V specimens produced by shaped metal deposition. Sci Technol Adv Mater 10:1–10
7. Tabernero I, Lamikiz A, Martínez S et al (2011) Evaluation of the mechanical properties of Inconel 718 components built by laser cladding. Int J Mach Tool Manu 51:465–470
8. Skiba T, Baufeld B, Biest O (2009) Microstructure and mechanical properties of stainless steel component manufactured by shaped metal deposition. ISIJ Int 49(10):1588–1591
9. Skiba T, Baufeld B, Van der Biest O (2011) Shaped metal deposition of 300M steel. P I Mech Eeg B-J Eng 225(6):831–839
10. Ouyang JH, Wang H, Kovacevic R (2002) Rapid prototyping of 5356-aluminum alloy based on variable polarity gas tungsten arc welding: process control and microstructure. Mater Manuf Process 17(1):103–124
11. Wang H, Kovacevic R (2000) Variable polarity GTAW in rapid prototyping of aluminum parts. Proceedings of the 11th Annual Solid Freeform Fabrication Symposium, Austin, TX, 369–376
12. Liu YB, Sun QJ, Jiang YL (2014) Rapid prototyping process based on cold metal transfer arc welding technology. Trans China Weld Inst 35:1–4
13. Mullins WW, Sekerka RF (1964) Stability of a planar interface during solidification of a dilute binary alloy. J Appl Phys 35(2): 444–451
14. Howe A (2002) Rationalisation of interstitial diffusion. Scripta Mater 47(10):663–667

15. Tiller WA, Jackson KA, Rutter JW, Chalmers B (1953) The redistribution of solute atoms during the solidification of metals. Acta Metall 1(4):428–437
16. Steward PA (1998) Fick's laws of diffusion
17. Poirier DR, Yeum K, Maples AL (1987) A thermodynamic prediction for microporosity formation in aluminum-rich Al-Cu alloys. Metall Trans A 18(11):1979–1987
18. Mazur M (1992) Porosity in aluminium welds. Weld Int 6(12):929–931